UC Irvine

Title

Visual restoration and transplant connectivity in degenerate rats implanted with retinal progenitor sheets

Permalink

https://escholarship.org/uc/item/2np3192b

Journal

European Journal of Neuroscience, 31(3)

ISSN

0953-816X

Authors

Seiler, MJ
Aramant, RB
Thomas, BB
et al.

Publication Date

2010-02-01

DOI

10.1111/j.1460-9568.2010.07085.x

Peer reviewed

NEUROSYSTEMS

Visual restoration and transplant connectivity in degenerate rats implanted with retinal progenitor sheets

M. J. Seiler,[1,2,3] R. B. Aramant,[1] B. B. Thomas,[2] Q. Peng,[2,4] S. R. Sadda[2] and H. S. Keirstead[1]

[1]Reeve-Irvine Research Center, Sue and Bill Gross Stem Cell Research Center, 2111 Gillespie Neuroscience Research Facility, School of Medicine, University of California at Irvine, Irvine, CA 92697-4292, USA
[2]Ophthalmology, Doheny Eye Institute, Keck School of Medicine, USC, Los Angeles, CA, USA
[3]Cell & Neurobiology, Keck School of Medicine, USC, Los Angeles, CA, USA
[4]Ophthalmology, School of Medicine, Shanghai Jiao Tong University, Shanghai, China

Abstract

The aim of this study was to determine whether retinal progenitor layer transplants form synaptic connections with the host and restore vision. Donor retinal sheets, isolated from embryonic day 19 rat fetuses expressing human placental alkaline phosphatase (hPAP), were transplanted to the subretinal space of 18 S334ter-3 rats with fast retinal degeneration at the age of 0.8–1.3 months. Recipients were killed at the age of 1.6–11.8 months. Frozen sections were analysed by confocal immunohistochemistry for the donor cell label hPAP and synaptic markers. Vibratome slices were stained for hPAP, and processed for electron microscopy. Visual responses were recorded by electrophysiology from the superior colliculus (SC) in 12 rats at the age of 5.3–11.8 months. All recorded transplanted rats had restored or preserved visual responses in the SC corresponding to the transplant location in the retina, with thresholds between −2.8 and −3.4 log cd∕m². No such responses were found in age-matched S334ter-3 rats without transplants, or in those with sham surgery. Donor cells and processes were identified in the host by light and electron microscopy. Transplant processes penetrated the inner host retina in spite of occasional glial barriers between transplant and host. Labeled neuronal processes were found in the host inner plexiform layer, and formed apparent synapses with unlabeled cells, presumably of host origin. In conclusion, synaptic connections between graft and host cells, together with visual responses from corresponding locations in the brain, support the hypothesis that functional connections develop following transplantation of retinal layers into rodent models of retinal degeneration.

Introduction

Diseases of the outer retina, such as age-related macular degeneration (Zarbin, 2004; Jager *et al.*, 2008) and retinitis pigmentosa (Kalloniatis & Fletcher, 2004; Kennan *et al.*, 2005), affect over 12 million people in the USA alone. In these diseases, photoreceptors and∕or the retinal pigment epithelium are dysfunctional and degenerate. However, the remaining inner neural retina that connects to the brain can still remain functional (Papermaster & Windle, 1995; Santos *et al.*, 1997; Milam *et al.*, 1998; Humayun *et al.*, 1999), although significant remodeling occurs over time (Strettoi *et al.*, 2003; Marc *et al.*, 2007). If the diseased cells can be replaced with new cells that can make appropriate and functional connections with the host retina, a degenerated retina might be repaired and eyesight restored.

Transplantation of freshly isolated retinal progenitor sheets improves and preserves, in different retinal degeneration models, visual responses in the superior colliculus (SC) that cannot be seen with sham surgery or in age-matched controls (Woch *et al.*, 2001;

Sagdullaev *et al.*, 2003; Arai *et al.*, 2004; Thomas *et al.*, 2004, 2006). Synaptic connections between the transplant and the degenerated host retina have been indicated by trans-synaptic tracing studies (Seiler *et al.*, 2005). In addition, it has been demonstrated that visual responses in the SC can be traced back to retinal transplants in the subretinal space (Seiler *et al.*, 2008b). However, direct synaptic connections have not been conclusively demonstrated ultrastructurally.

This study investigated transplant–host connectivity of retinal sheet transplants in a rat model of retinal degeneration. Our data indicate that transplanted rats had restored or preserved visual responses in the SC. Importantly, visual restoration was correlated with the presence of donor cells and processes that penetrated the host inner plexiform layer, and formed synapses with the host.

Materials and methods

Experimental animals

For all experimental procedures, animals were treated in accordance with the NIH guidelines for the care and use of laboratory animals and the ARVO Statement for the Use of Animals in Ophthalmic and

Vision Research, and under a protocol approved by the Institutional Animal Care and Use Committee of the Doheny Eye Institute, University of Southern California. Eighteen transgenic pigmented S334ter-3 retinal degenerate rats expressing a mutated human rhodopsin protein (Sagdullaev *et al.*, 2003) received retinal sheet transplants in one eye at postnatal day 24–38. Of these, 12 animals were selected for recording of visual responses in the SC (Table 1).

Most of the procedures used in these experiments have been described in detail elsewhere (Woch *et al.*, 2001; Sagdullaev *et al.*, 2003; Thomas *et al.*, 2004).

Donor tissue

Transgenic rats carrying the human placental alkaline phosphatase (hPAP) gene (Kisseberth *et al.*, 1999) were used as the source of donor tissue. Rats expressing both green fluorescent protein and hPAP were used as donors for eight of the 18 experiments, and were derived from a cross between hPAP and green fluorescent protein transgenic rats (Hakamata *et al.*, 2001). Rat mating was confirmed by vaginal smears. At day 19 of gestation (day of conception = day 0), fetuses were removed by Cesarean section after terminal anesthesia with an overdose of Na-pentobarbital (240 mg/kg, i.p.) Small pieces of the fetuses' tails or limbs were tested by histochemistry for hPAP (Kisseberth *et al.*, 1999) to identify transgenic fetuses. Embryos were stored in Hibernate E medium (Brainbits, Springfield, IL, USA) with B-27 supplements (InVitrogen, Carlsbad, CA, USA) for up to 6 h. The retinal tissue was flattened in a drop of medium. Retinal progenitor sheets were cut into rectangular pieces of $1–1.5 \times 0.6$ mm to fit into a previously described custom-made implantation tool (Seiler &

Aramant, 1998; Aramant & Seiler, 2002). Immediately before implantation, the tissue was taken up in the correct orientation (ganglion cell side up) into the flat nozzle of the implantation tool.

In nine of 18 experiments (Table 1), retinal sheets were incubated in brain-derived neurotrophic factor microspheres for at least 1 h before transplantation (Mahoney & Saltzman, 2001; Seiler *et al.*, 2008a).

Transplant recipients

Transgenic pigmented S334ter-3 rhodopsin mutant rats were used as graft recipients at the age of 26–38 days. The rats were originally produced by Xenogen Biosciences (formerly Chrysalis DNX Transgenic Sciences, Princeton, NJ, USA), and developed and supplied with the support of the National Eye Institute by M. LaVail, University of California San Francisco (http://www.ucsfeye.net/mlavailRDratmodels.shtml). Recipients were the F_1 generation of a cross between albino homozygous S334ter-3 and pigmented Copenhagen rats (Harlan, Indianapolis, IN, USA).

Transplantation surgery

S334ter-3 rats were anesthetized by intraperitoneal injection of a mixture of 37.5 mg/kg ketamine and 5 mg/kg xylazine in sterile saline, and their pupils were dilated by 1% atropine sulfate. A small incision (approximately 1 mm) was cut behind the pars plana. A custom-made implantation tool (US patent #6 159 218) was loaded with a retinal progenitor sheet and placed into the subretinal space in the superior nasal quadrant of the host retina. Then, the donor tissue was slowly and gently released. The scleral incision was closed with

TABLE 1. Overview of experiments

Rat no.	Donor tissue	Age at surgery (months)	Age at death (months)	Time after surgery (months)	Visual threshold at SC recording (log cd/m^2)	Method of analysis
1	E19 retina + BDNF	0.9	1.6	0.7	NA	EM
2*	E19 retina + BDNF	0.8	2.8	2.0	NA	EM
3	E19 retina + BDNF	1.2	5.3	4.1	−3.4	EM
4	E19 retina	1.1	5.4	4.3	−2.8	EM
5*	E19 retina	1.1	5.4	4.3	−2.8	EM
6	E19 retina + BDNF	0.9	6.9	6.1	−2.8	EM
7	E19 retina + BDNF	0.9	7.6	6.7	−2.8	EM
8	E19 retina	1.0	8.9	8.0	NA	EM
9	E19 retina	1.0	8.9	8.0	NA	EM
10	E19 retina	1.0	10.1	9.1	NA	EM
11	E19 retina + BDNF	1.3	11.6	10.3	−2.8	EM
12	E19 retina + BDNF	1.3	11.7	10.5	−2.8	EM
13	E19 retina + BDNF	1.3	11.8	10.5	−2.2	EM
14	Sham surgery	1.0	2.7	1.6	No response	LM
15	Sham surgery	0.8	3.1	2.3	No response	LM
16	Sham surgery	1.1	5.4	4.2	−0.4	LM
17	E19 retina	0.9	3.0	2.1	−3.4	Confocal
18	E19 retina	0.9	3.0	2.1	−2.8	Confocal
19	E19 retina + BDNF	0.9	3.0	2.1	−2.8	Confocal
20	E19 retina	0.9	3.1	2.2	−2.8	Confocal
21	E19 retina	0.8	3.5	2.7	Not recorded	Confocal
Summary (*n* = 21 rats) 9 retina + BDNF, 9 retina only, 3 sham surgery		0.8–1.3	1.6–11.8	0.7–10.5	15 of 21 recorded	

Experiments are ordered according to age at death and time post-surgery. Slices of rats 6–13 were processed for gold–silver toning after human placental alkaline phosphatase (hPAP) immunostaining. '+ BDNF' indicates that donor tissue was incubated with BDNF containing microspheres before transplantation. Rats 14–16 (sham surgery) and 17–21 were only processed for light microscopy (rats 17–21 were studied by confocal immunohistochemistry). BDNF, brain-derived neurotrophic factor; E, embryonic day; EM, electron microscopy; LM, light microscopy; NA, not applicable; SC, superior colliculus. *Histology of rats 2 and 5 was shown in Peng *et al.* (2007), without silver–gold toning of hPAP immmunostaining. For the current study, additional slices were immunostained for hPAP with silver–gold toning and processed for EM.

10–0 sutures. Immediately following the surgery, the fundus of the rat was examined by a contact lens on the cornea to identify the transplant placement. The eyes were treated with gentamicin ointment. Rats recovered from anesthesia in an incubator before they were returned to their cage. As a control, other rats received injections of medium into the subretinal space, with the same instrument and nozzle (sham surgery).

SC recording

Electrophysiological assessment of visual responses in the SC was performed in 15 of the 21 rats, according to a method described previously (Thomas *et al.*, 2005). Rats were dark-adapted overnight. Animals were initially anesthetized by intraperitoneal injection of ketamine/xylazine (37.5 mg/kg ketamine and 5 mg/kg xylazine), and subsequently by a gas inhalant anesthetic (1.0–2.0% halothane in 40% O_2/60% N_2O) administered via an anesthetic mask (Stoelting Company, Wood Dale, IL, USA). The surface of the right SC was exposed by suction. The eyes were covered with a custom-made eye-cap to prevent bleaching of the photoreceptors during the surgery, and the eye-cap was removed for visual stimulation. Using nail polish-coated tungsten microelectrodes, multi-unit visual responses were recorded extracellularly from the superficial laminae of the exposed SC. At each recording location, up to 16 presentations of a full-field illumination (controlled by a camera shutter) were projected onto a white Plexiglas screen placed 10 cm in front of the contralateral eye. The intensity of the light stimulus at the beginning of the recording was -6.46 log cd/m^2, and it was gradually increased (controlled by neutral density filters) until the visual threshold was measured. An interstimulus interval of 6 s was used. All electrical activity was recorded using a digital data acquisition system (Powerlab; ADI Instruments, Mountain View, CA, USA), and responses (8–16 sweeps) at each SC site were averaged using MATLAB software (R2006b). Blank trials, in which the illumination of the eye was blocked with an opaque filter, were also performed. As a control, age-matched non-transplanted S334ter-3 rats, rats with sham surgery and normal pigmented Long-Evans rats underwent the same recording protocol as transplanted rats.

Tissue processing

After terminal anaesthesia with Na-pentobarbital (240 mg/k.g. i.p.) were perfusion-fixed through the ascending aorta with a mixture of 4% paraformaldehyde and 0.1–0.4% glutaraldehyde in 0.1 M sodium phosphate buffer (pH 7.2). The eyes were enucleated, the anterior segment was removed, and the posterior eye-cup was postfixed in the same fixative overnight at 4°C. After washing of the eye-cups several times with 0.1 M sodium phosphate buffer (PB), the eye-cup area containing the transplant was dissected along the dorsoventral axis, and subjected to one of the following procedures: infiltration with 30% sucrose overnight, embedding in Optimal Cutting Temperature compound (Sakura Finetek USA, Torrance, CA, USA), and freezing in isopentane on dry ice for cutting of 10-μm cryostat sections; or embedding in 4% agarose in 0.1 M PB for vibratome sectioning at 80 μm.

Confocal double-label immunohistochemistry for hPAP and synaptic markers

Cryostat sections were processed for immunohistochemistry using established methods (e.g. Seiler *et al.*, 2008a). After being washed with phosphate-buffered saline (PBS; 0.1 M NaCL, 0.01 M sodium

phosphate buffer, pH 7.2), sections were incubated in 10% goat serum for at least 1 h for blocking, and then incubated in a mixture of primary antibodies overnight at 4°C. After several PBS washes, sections were incubated for 30–60 min with an appropriate mixture of secondary goat antibodies directed against mouse or rabbit IgG, diluted 1 : 200 in blocking serum, and tagged with either AF488 or Rhodamine Red X (Molecular Probes). After further washes, slides were mounted with 4′,6′-diamidino-2-phenylindole hydrochloride-containing mounting medium (Vectashield; Vector Labs, Burlingame, CA, USA).

For detection of the hPAP donor tissue, a monoclonal mouse antibody, 8B6 (Chemicon, Temecula, CA, USA), was used at a dilution of 1 : 400 to 1 : 500 in combination with the following rabbit antisera: anti-metabotropic glutamate receptor 6 (mGluR6) (1 : 200; Neuromics, Edina, MN, USA); and anti-synapsin 1 (1 : 500; Chemicon). Alternatively, a rabbit monoclonal antibody against hPAP was used (clone SP15; 1 : 50; Epitomics, Burlingame, CA, USA); this required antigen retrieval of dried frozen sections for 20 min at 70°C using HistoVT One (Nacalai USA Inc., San Diego, CA, USA), followed by three washes in PBS and incubation in blocking serum. The following monoclonal mouse antibodies were used in combination with the rabbit SP15 antibody: anti-synaptophysin (1 : 5000; Sigma, St Louis, MO, USA); anti-bassoon (1 : 600; Stressgen, Ann Arbor, MI, USA); anti-PSD95 (1 : 500; Stressgen); and anti-syntaxin 1 (HPC-1; 1 : 500) (Barnstable *et al.*, 1985) (gift of C.J. Barnstable, now at Penn State College of Medicine, Hershey, CA, USA). As control, primary antibodies were omitted.

Sections were imaged using a Zeiss LSM710 confocal microscope. Stacks were created from 7–12 slices at different focal levels (0.36 μm apart), and analysed with ZEN software (ZEN 2008 light edition; Carl Zeiss MicroImaging, Inc., Thornwood, NY, USA). Images (separate for each color channel) were exported and combined in ADOBE PHOTOSHOP CS.

Immunohistochemistry for hPAP on vibratome slices

Selected vibratome sections were washed five times for 10 min in 0.1 M PB, and then incubated for 15 min in 1% sodium borohydride (NaBH$_4$) in 0.1 M PB. After being washed five times for 10 min each, the sections were treated for 30 min in 50% ethanol in PBS, and then subjected to three 10-min PB washes. Vibratome sections were washed with PBS, and incubated for 2 h in 10% goat serum in PBS/1% bovine serum albumin. The sections were incubated at 4°C with different mouse monoclonal antibodies against hPAP antigen, and diluted in blocking serum, under continuous rotation: clones MAB102 (1 : 5000; Chemicon) and 8B6 (1 : 1000, 1 : 2000; Chemicon; Sigma; Cymbus Biotech, Eastleigh, UK) were used. After 72 h, sections were incubated in a 1 : 200 dilution of biotin-conjugated goat anti-mouse IgG (Chemicon) for 18–24 h at 4°C. Controls included slices that were incubated without primary antibody, and slices that did not contain any transplant (either from non-surgery eyes or from outside the transplant area) that were incubated with hPAP antibodies. After being washed five times for 10 min each with PBS, slices were incubated overnight at 4°C in Elite ABC conjugated to horseradish peroxidase (Vector Labs). After being subjected to five 10-min washes with PBS, sections were stained for peroxidase activity by incubation in a diaminobenzidine tetrahydrochloride (DAB) substrate kit (Vector Labs). The DAB reaction was stopped at 5–7 min by five 10-min washes in PBS, followed by placement in 0.05 M Tris–HCl buffer. Sections were then exposed to silver–gold toning according to the protocol of Teclemariam-Mesbah *et al.* (1997): (i) 3×10 min sodium acetate 2%; (ii) incubation in a freshly made solution consisting of

150 mL of 3% methenamine, 20 mL of 5% silver nitrate and 20 mL of 1% sodium tetraborate for 5 min at 60°C; (iii) 3 × 10 min sodium acetate 2%; (iv) 5 min 0.1% gold chloride; (v) 3 × 10 min sodium acetate 2%; (vi) 5 min sodium thiosulfate 3%; (vii) 3 × 10 min sodium acetate 2%; and (viii) 3 × 10 min rinse in PBS.

Electron microscopy

Selected slices were washed five times with 0.1 M cacodylate buffer, postfixed with 3% glutaraldehyde with 0.1 M cacodylate buffer, washed five times with 0.1 M cacodylate buffer again, osmicated (1% osmium in 0.1 M cacodylate buffer), stained *en bloc* in 1% uranyl acetate in 50 mM sodium acetate buffer (pH 5.2) overnight, and then processed for Epon embedding and electron microscopy. Semithin and ultrathin sections (70 nm thick) were cut with a diamond knife. For electron microscopy, semithin sections were cut until the transplant–host interface was clearly identifiable, and ultrathin sections were then cut. Sections were not counterstained. Sections were viewed in either a Philips CM10, a Zeiss EM10 or a JEOL1400 electron microscope. Synapses were identified at magnifications above ×7500 by the presence of synaptic vesicles on the presynaptic side and the presence of postsynaptic density on the postsynaptic side.

Quantification of electron microscopic staining

In selected images of the host inner plexiform layer (magnification range between ×3000 and ×11 500; 21 hPAP-stained images of seven animals, and 11 control images of three animals), silver grains were counted by two independent observers. Electron microscopic images of immunostained slices were selected on the basis of their content of stained regions; control images were selected randomly from control samples (controls included omission of primary antibody, host retina outside transplant on stained slice, and stained slice of non-surgery eye). Silver grain densities (silver grains/μm^2) were statistically compared using GRAPHPAD Version 3.05 software (GraphPad, San Diego, CA, USA) (unpaired *t*-test with Welch correction).

Results

Visual responses in the SC

Fifteen transplanted rats with clear corneas and lenses were selected for electrophysiological evaluation of the visual responses. All rats showed visual responses to low-light stimulation (−3.42 to −2.8 log cd/m^2) in a small area of the SC corresponding to the placement of the transplant in the retina (Table 1). Representative examples of traces recorded at different light intensities from the SC of a normal pigmented Copenhagen rat, a 3-month-old non-surgery S334ter-3 rat and 5-month-old sham surgery and transplanted S334ter-3 rats are shown in Fig. 1. Responses recorded from the transplanted rats had comparatively longer latencies than those of normal pigmented rats, and they had higher background activity than those of normal rats. No responses were found in age-matched or younger S334ter-3 rats without surgery or with sham surgery at or below a light intensity of −1.0 log cd/m^2.

Transplant organization (light microscopy)

Eight of the 18 transplants contained laminated areas (examples are given in Figs 2–4) with photoreceptor outer segments in the correct orientation in contact with the host retinal pigment epithelium

(Fig. 4C). All 18 transplants contained areas with photoreceptors in rosettes (arranged in spheres with outer segments in the center of the rosette, surrounded by inner retinal layers) (examples are given in Figs 3B, 2, and 4B).

Confocal analysis of immmunostaining for hPAP and synaptic markers

Figures 2 and 3 show examples of staining of rat 17, using a combination of mouse or rabbit antibodies with rabbit anti-synapsin 1, mouse anti-syntaxin (HPC-1), anti-synaptophysin (Fig. 2), rabbit anti-mGluR6, mouse anti-bassoon, and anti-PSD95 (Fig. 3). hPAP staining with either the mouse antibody 8B6 or the rabbit antibody SP15 consistently showed extension of transplant processes past remnants of host cones into the host inner nuclear and inner plexiform layers. Most of these processes were neuronal, as they showed double staining for synaptic markers. Processes in the transplant–host interface partially colocalized with the synaptic markers synapsin 1 (Fig. 2A), syntaxin (HPC-1) (Fig. 2B), synaptophysin (Fig. 2C), and mGluR6 (Fig. 3A), indicating that they contained presynaptic and postsynaptic elements. Transplant processes at the border between host inner nuclear layer and inner plexiform layer appeared to be postsynaptic, as seen with bassoon staining (Fig. 3B2 and B3). PSD95 staining showed several presynaptic transplant processes adjacent to PSD95-immunoreactive processes in the host outer plexiform layer (Fig. 3C). Because of the dense staining of synapses in the host inner plexiform layer with the antibodies against synapsin, syntaxin, synaptophysin and bassoon, it was impossible to determine whether transplant processes in the host inner plexiform layer were presynaptic or postsynaptic. Similar results were seen in rats 18–21 (data not shown).

Controls in which primary antibodies were omitted did not show any staining (data not shown).

hPAP staining of vibratome slices (light microscopy)

hPAP immunoreactivity was found up to 10 μm from both surfaces of the vibratome slices, clearly showing the cytoplasm of the donor tissue (examples are given in Fig. 4A, C1, C2 and D). Thus, when the surface of the slice was unevenly oriented, only partial staining was visible (examples are given in Fig. 4C and D). Transplants could be observed extending processes into the host inner nuclear layer, and many hPAP-immunoreactive processes could be observed in the inner plexiform layer overlying the transplant (an example is given in Fig. 4D). No comparable staining was observed in controls in which the primary antibody was omitted (Fig. 4E), or in eyes without a transplant (Fig. 2F), although there was some non-specific marginal staining in the ganglion cell layer close to the retinal surface. Outside the transplant area, no hPAP immunoreactivity was observed in the host inner plexiform layer (Fig. 4G).

hPAP staining (electron microscopy)

After gold–silver toning, hPAP immunoreactivity could be identified as silver grains of varying sizes (Figs 6 and 7), which were much easier to clearly identify in the electron microscope than the DAB precipitate in experiments without silver–gold toning [data not shown; see Peng *et al.* (2007)].

In control slices in which the primary antibody was omitted (Fig. 5A–C), and in non-transplanted eyes that had been stained for hPAP (Fig. 5D–I), only low concentrations of silver grains were found. Unspecific silver grains were mainly observable as edge
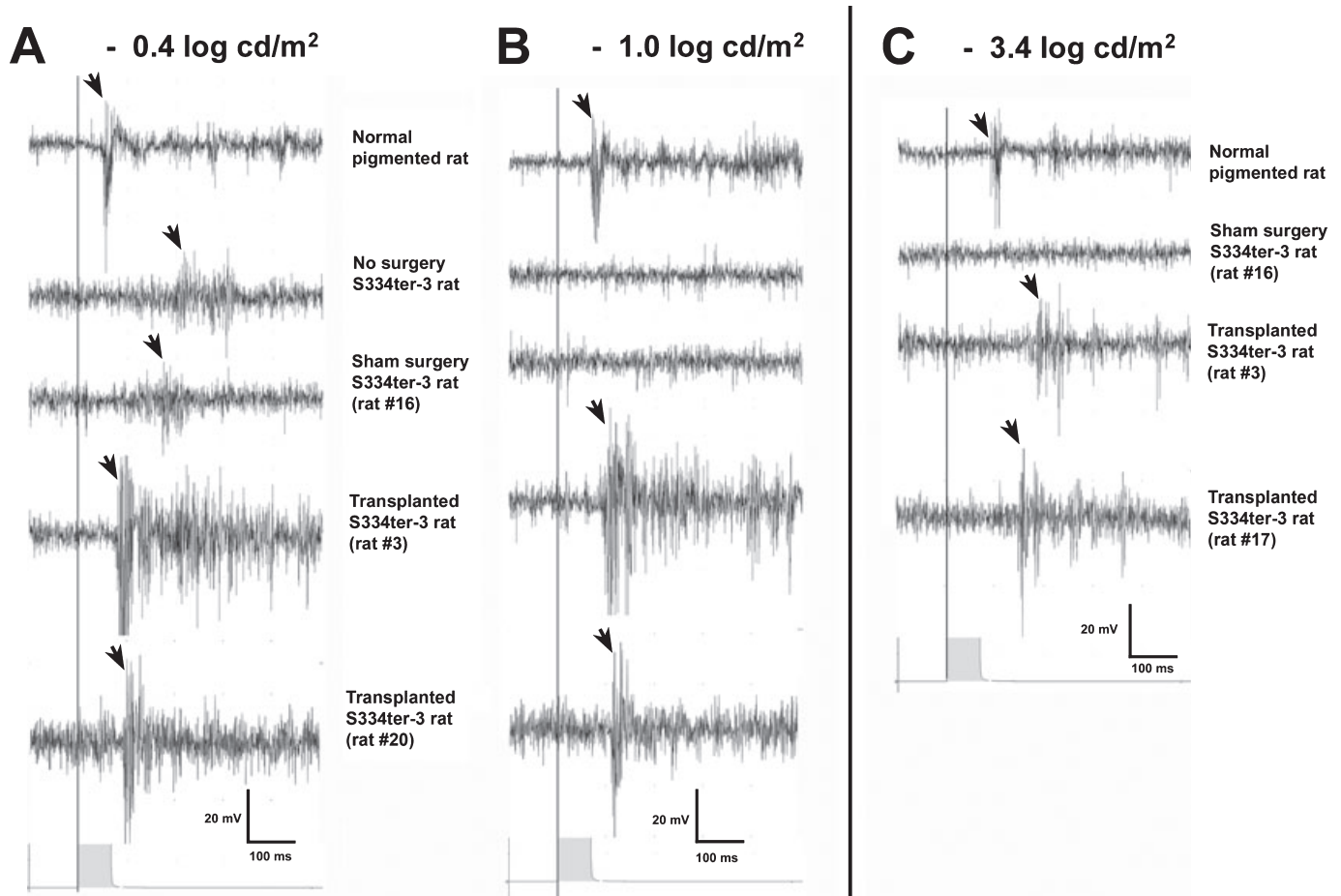
FIG. 1. Examples of superior colliculus recordings at different light intensities: normal pigmented rat; S334ter-3 rat without surgery (age 3 months); sham surgery rat 16 (age 5.4 months); retinal transplant rats 3 (age 5.3 months), 17 and 20 (age 3.0–3.1 months). The light stimulus (duration 85 ms) is indicated at the bottom of each panel. The onset of light responses is indicated by arrows. (A) At a light intensity of −0.4 log cd/m², faint responses with low amplitudes and long latencies can be seen for the non-surgery and sham surgery S334ter-3 rats, whereas the transplanted rats (3 and 20) show a robust response in one area that is only slightly delayed as compared with normal. Transplanted rats show more noisy background activity. (B) At the slightly reduced light intensity of −1.0 log cd/m², no responses can be observed in the non-surgery and sham surgery S334ter-3 rats, whereas the response from the transplant rats (3 and 20) remain robust. (C) At a much reduced light intensity of −3.4 log cd/m², there is no response in the sham surgery rat. In the transplant rats (3 and 17) there are still clear responses, although with a much longer latency than in the normal rat. [Rat 20 had a response threshold of −2.8 log cd/m² (not shown) and did not respond at this light intensity.]

staining outside the tissue (Fig. 5A), or as random accumulations inside the tissue (Fig. 5D–I). The unspecific stain was clearly different from the specific stain shown in Figs 6 and 7. A significant difference in silver grain densities was observed between stained images and controls (Fig. 5J).

Examples of staining at the transplant–host interface are shown in Fig. 6. Donor-derived processes could be observed penetrating the inner nuclear layer of the host retina (Fig. 6A–D), sometimes forming close, potentially synaptic, contacts with unlabeled cells, presumably belonging to the host (Fig. 6D–F).

In the inner plexiform layer of the host retina, many hPAP-immunoreactive neuronal processes could be observed in all experiments (Fig. 7). The extent and density of processes varied between experiments (Fig. 7). In many instances, labeled processes made apparent synapses with unlabeled host cells (Fig. 7A–F). Most synapses appeared to be conventional; ribbon synapses could be observed rarely (Fig. 7A). Labeled processes were found both on the presynaptic side (Fig. 7A, D and E) and on the postsynaptic side (Fig. 7B, C and F) of synapses. The hPAP label obscured some of the synaptic structures. The resolution of membranes was not comparable to that of tissue processed for conventional electron microscopy, because of the difference in fixation and the lack of counterstain with lead citrate.

Discussion

This study documents, for the first time, direct evidence at the ultrastructural level for synaptic connectivity between retinal progenitor sheet transplants and degenerating host retinas, and provides further evidence that synaptic connectivity between graft and host plays an important role in transplant-mediated visual restoration. These findings confirm and extend our previous observations of restored visual function (Woch *et al.*, 2001; Sagdullaev *et al.*, 2003; Thomas *et al.*, 2004) and synaptic connectivity shown by trans-synaptic tracing (Seiler *et al.*, 2005, 2008b) of retinal sheet transplants in rodent models of retinal degeneration.

In all cases, retinal sheet transplants restored responses to mesopic light stimulation (−2.8 to −3.4 log cd/m²) in an area of the SC corresponding to the placement of the transplant in the retina (age up to 12 months; up to 10.5 months after transplantation). The transplant
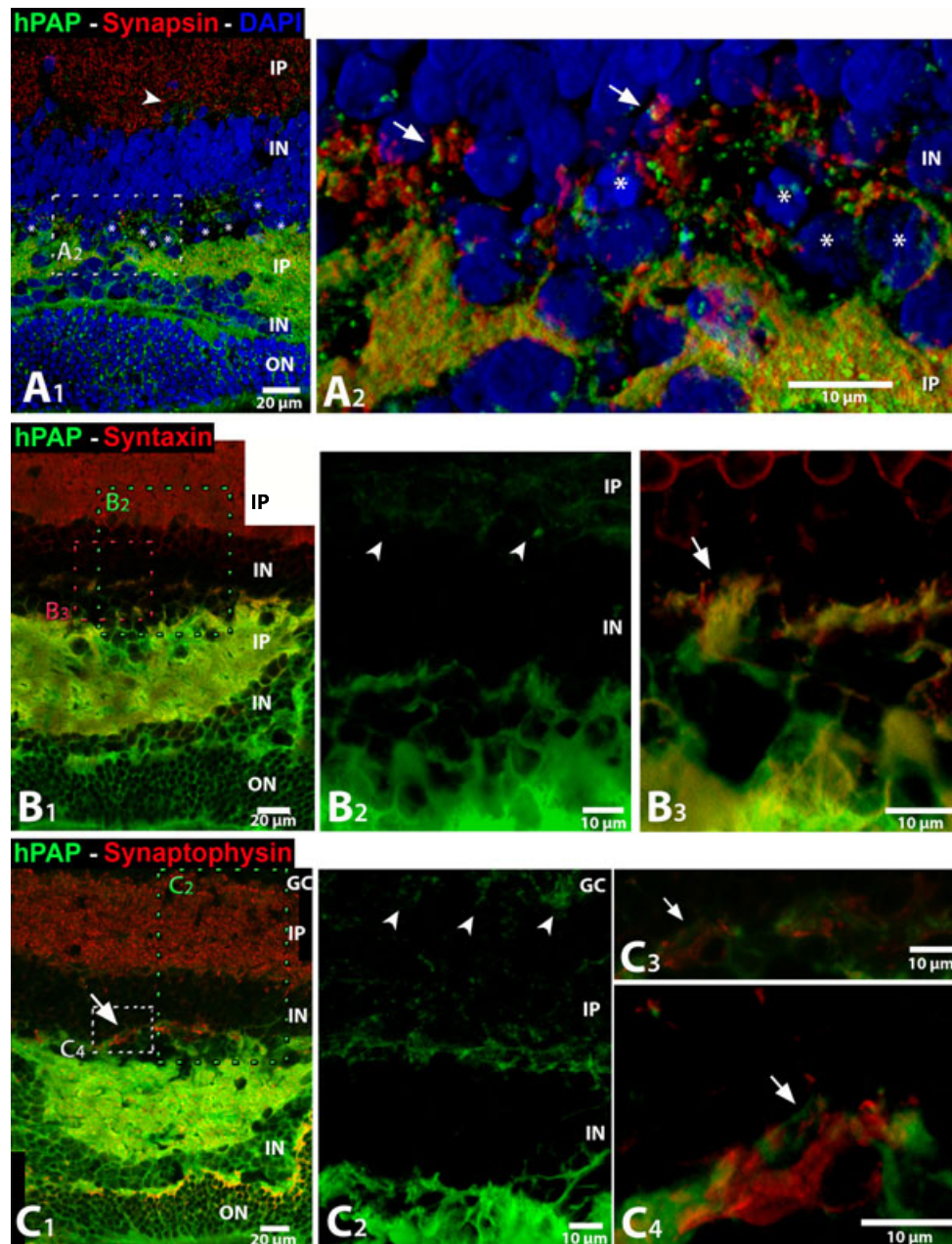
FIG. 2. Combination of donor cell label [human placental alkaline phosphatase (hPAP)] with the presynaptic markers synapsin, syntaxin (HPC-1), and synaptophysin (confocal imaging-see colour images on-line). All images are of rat 17. Similar images were obtained from rats 18–21. All images are oriented with the host ganglion cell layer (GC) up. White asterisks (*) indicate nuclei of remnant host cones (containing clumped chromatin). The cytoplasm, including processes of all transplant cells (not the nuclei), is labeled with hPAP (green). (A1 and A2) Combination of mouse anti-hPAP (8B6, green) and rabbit anti-synapsin (red, marker for synaptic vesicles and synaptic terminals), and 4′,6′-diamidino-2-phenylindole hydrochloride (DAPI) nuclear label (blue). Both images are three-dimensional stacks. (A1) Overview. Transplant processes extend past remnants of host cones to the outer plexiform layerof the host. In addition, there are numerous hPAP-stained processes in the inner plexiform layer (IP) of the host, mostly obscured by the synapsin stain. The arrowhead points to a group of processes that is visible at this level. The white dashed box indicates enlargement in A2. (A2) Enlargement of the transplant–host interface. Examples of areas with potential transplant–host synaptic interactions (transplant processes close to red-stained synaptic structures outside transplant) are indicated by arrows. The black space in the transplant–host interface is a cutting artefact. (B1–B3) Rabbit anti-hPAP (SP15) (green) in combination with mouse anti-syntaxin (HPC-1) (red). Syntaxin stains synaptic layers and somas of amacrine cells. (B1) Overview of transplant. Composition of two single slices at the same focus level. Note the overlap of red and green channels in the transplant–host interface. The box with green dashes indicates the area shown in B2; the box with red dashes indicates the area shown in B3. (B2) Three-dimensional stack of the transplant–host interface, showing hPAP staining (green channel). Transplant processes are extending into the host inner nuclear layer (IN). Numerous fine processes can be seen in the host inner plexiform layer (arrowheads). (B3) Greater enlargement of the transplant–host interface; three-dimensional stack of red and green channels. The arrow points to colocalization of hPAP and syntaxin in transplant processes. (C1–C4) Rabbit anti-hPAP (SP15) (green) in combination with mouse anti-synaptophysin (red, marker for synaptic vesicles) (slide adjacent to Fig. 2B). (C1) Overview of transplant. Projection of the stack at several focus levels. The box with green dashes indicates the area shown in C2; the box with white dashes indicates the area shown in C4. The arrow points to the area enlarged in C3. (C2) Three-dimensional stack of the transplant–host interface; hPAP staining (green channel). The arrowheads point to transplant processes close to the host ganglion cell layer. Note the transplant process extending into the host inner nuclear layer on the right side. (C3) Enlargement of the transplant–host interface in C1; single slice. The arrow points to a transplant process in contact with a synaptophysin-immunoreactive process, presumably from the host. (C4) Three-dimensional stack of the same area at higher magnification, making it clear that the transplant process is indeed contacting a host-derived process (arrow). ON, outer nuclear layer. Bars: 20 μm (A1, A2, B1, and C1), 10 μm (B2, B3, and C2–C4).
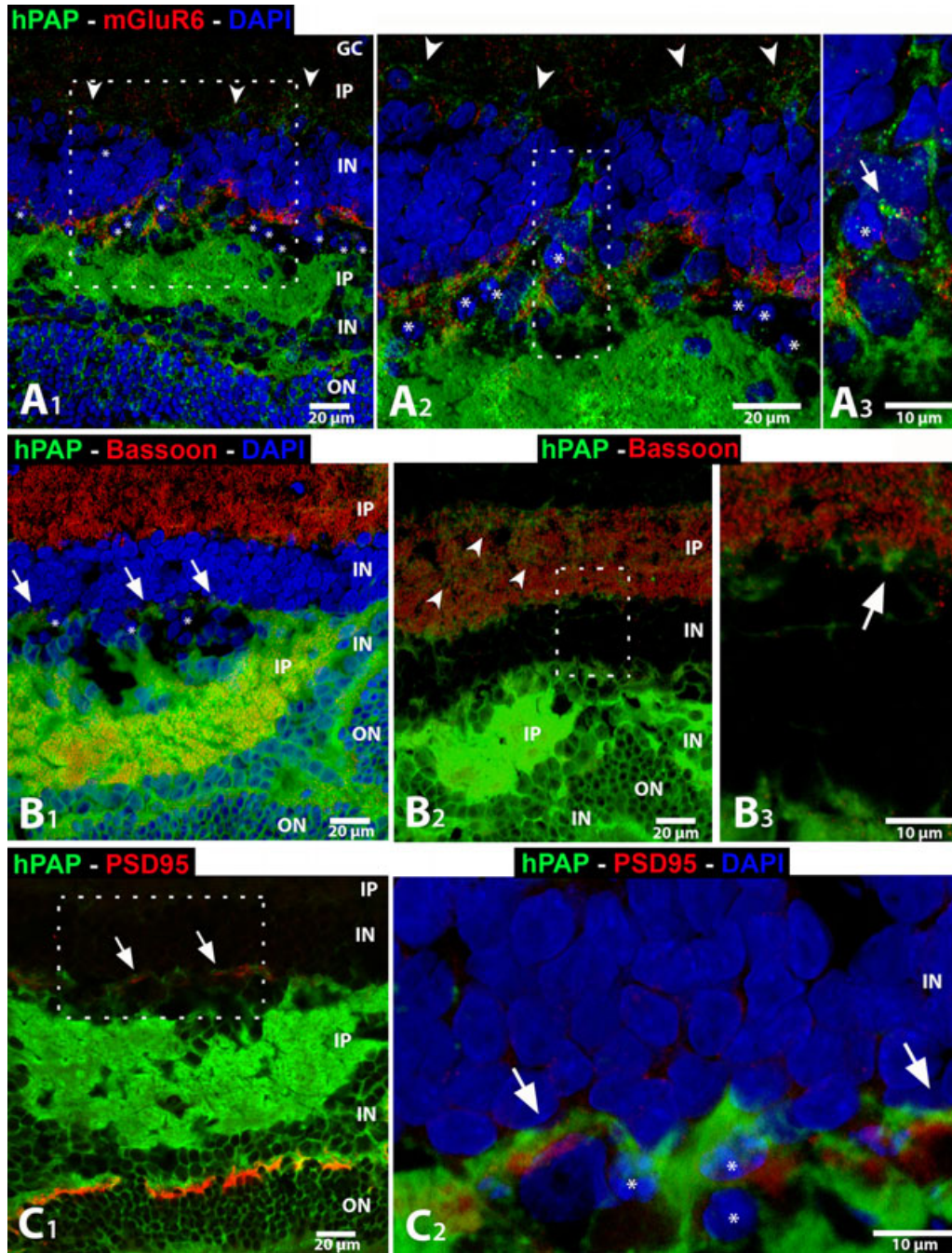
FIG. 3. Combination of donor cell label [human placental alkaline phosphatase (hPAP)] with the synaptic markers metabotropic glutamate receptor 6 (mGluR6), bassoon, and PSD95 (confocal imaging-see colour images on-line). All images are of rat 17. Similar images were obtained from rats 18–21. All images are oriented with the host ganglion cell layer (GC) up. White asterisks (*) indicate remnants of host cone nuclei with clumped chromatin. Black spaces at the transplant edge towards the host are cutting artefacts. (A1–A3) Combination of mouse anti-hPAP (8B6, green) with rabbit anti-mGluR6 (marker of synaptic terminals of on-bipolar cells; red); three-dimensional stack images (section adjacent to Fig. 2A). (A1) Overview. mGluR6 stains the dendritic tips of host and graft on-bipolar cells in the outer plexiform layer. Transplant processes extend past host cones, and penetrate the host inner nuclear layer (IN). There are also numerous processes in the host inner plexiform layer, close to the inner nuclear layer (arrowheads). The white dashed box indicates the area of enlargement in A2. (A2) Enlargement, showing the interaction between transplant processes and host on-bipolar cell dendritic tips. The white dashed box shows the area of enlargement in A3. (A3) Transplant process penetrating the host inner nuclear layer. The arrow points to a process double-stained for hPAP and mGluR6. (B1–B3) Rabbit anti-hPAP (SP15) (green) in combination with mouse anti-bassoon (marker for ribbon synapses, red) (section adjacent to Fig. 2B). (B1) Overview of the same area as in Fig. 2B. 4′,6′-Diamidino-2-phenylindole hydrochloride (DAPI) nuclear counterstain. Arrows point to the transplant–host interface in the host outer plexiform layer. Note the row of red dots indicating ribbon synapses in the outer plexiform layer of the host. Some of the dots are just outside, but close to, transplant processes. (B2) Adjacent area on the same section (red and green channel only), at a more disorganized transplant area where photoreceptors have rolled up into a rosette. Note numerous transplant processes in the host inner plexiform layer (IP) (arrowheads). The box indicates the area of enlargement in B3. (B3) The arrowhead points to a thick process at the border of the host inner nuclear and inner plexiform layers. (C1–C2) Rabbit anti-hPAP (SP15) (green) in combination with mouse anti-PSD95 (postsynaptic marker; red) (section adjacent to Figs 2B and 3B). (C1) Overview, single slice. Arrowheads point to transplant processes in contact with PSD95-immunoreactive processes in the host inner plexiform layer. (C2) Three-dimensional stack of the area in the white dashed box in C1. ON, outer nuclear layer. Bars: 20 μm (A1, A2, B1, B2, and C1), 10 μm (A3, B3, and C2).
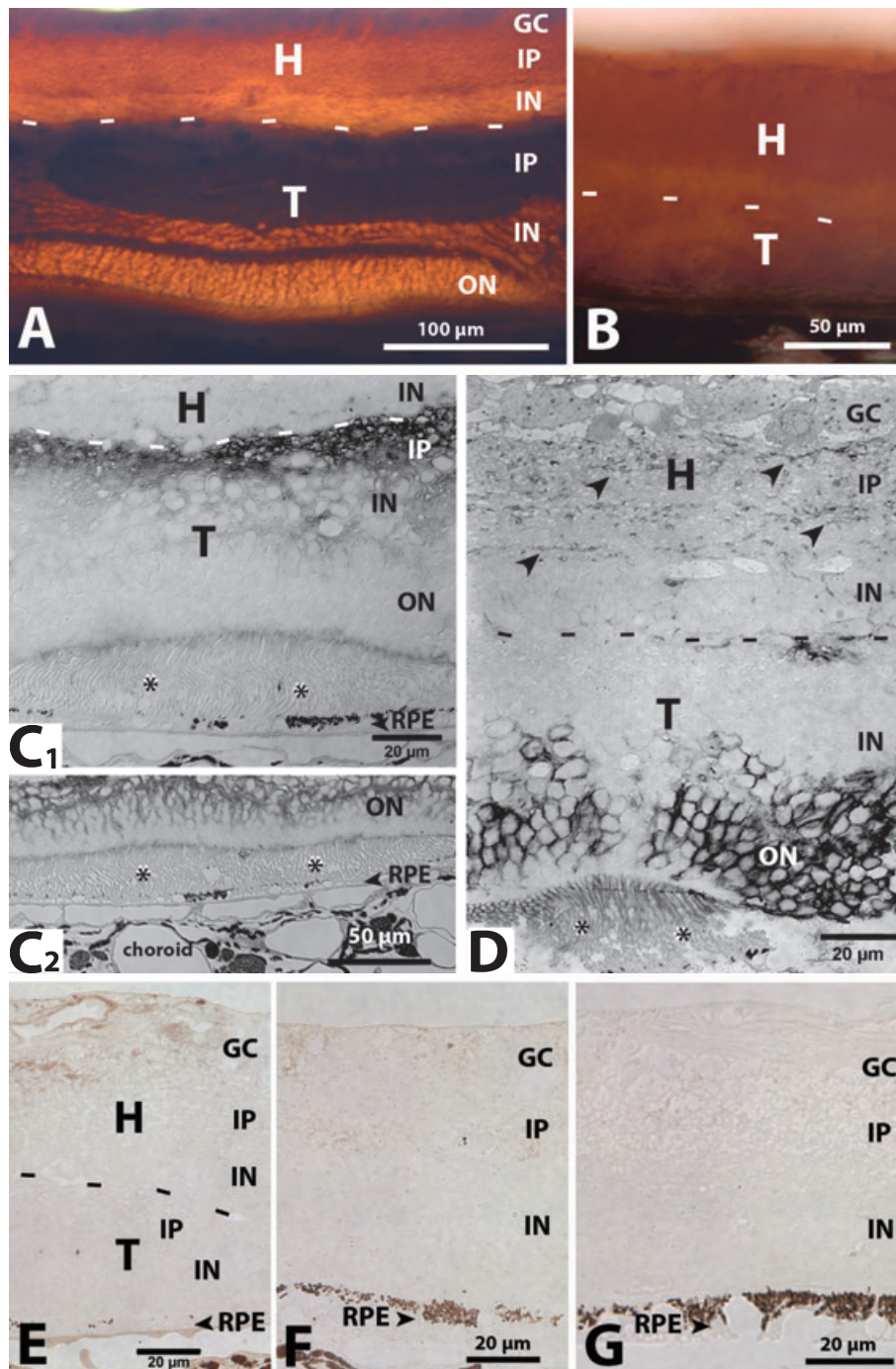
FIG. 4. Identification of the transplant by immunohistochemistry for human placental alkaline phosphatase (hPAP) – light microscopy. Dashes indicate the approximate transplant (T)–host (H) border, where applicable. (A) Vibratome slice, thickness 100 μm (rat 3), stained with monoclonal antibody 8B6 against hPAP (dilution 1 : 1000). The transplant inner plexiform layer (IP) and outer plexiform layer appear dark brown. (B) Control slice (rat 7), incubated with blocking serum instead of primary antibody, shows an even, light brown stain. (C) Example of stained vibratome slice (rat 5). This transplant has developed an area with photoreceptors in normal orientation and outer segments (indicated by asterisks,*). The diaminobenzidine tetrahydrochloride (DAB) stain penetrated the surface of the 80–100-μm-thick vibratome slices up to a depth of approximately 10 μm. Thus, if the surface of the tissue is unevenly oriented and sectioned, as seen in A and B, only partial staining is visible at a given sectioning level. (C1) DAB stain at the transplant–host interface. (C2) Stain of transplant photoreceptors was seen in previous sections of this slice. (D) Rat 1. DAB stain of transplant photoreceptors and in the host inner plexiform layer. The approximate border between transplant and host is indicated by dashes. Infiltration of the inner plexiform layer of the host retina by many labeled graft processes (examples indicated by arrowheads). The stained transplant–host interface had been seen in previous sections because the slice was not embedded perfectly flat. (E–G) Controls. (E) Section through a bcontrol slice of rat 7 that had been incubated with blocking serum instead of primary antibody. Non-specific edge staining in the ganglion cell layer (GC) and blood vessels is apparent, but no stain exists in the transplant. (F) Section through non-surgery fellow eye (degenerate retina without photoreceptor layer) of rat 13 without transplant. No stain. The retinal pigment epithelium (RPE) cells (arrowhead) contain black melanin granules. (G) Section of host retina outside transplant area (rat 9). No stain. IN, inner nuclear layer; ON, outer nuclear layer. Bars: 100 μm (A), 50 μm (B and C2), 20 μm (C1 and E–G).
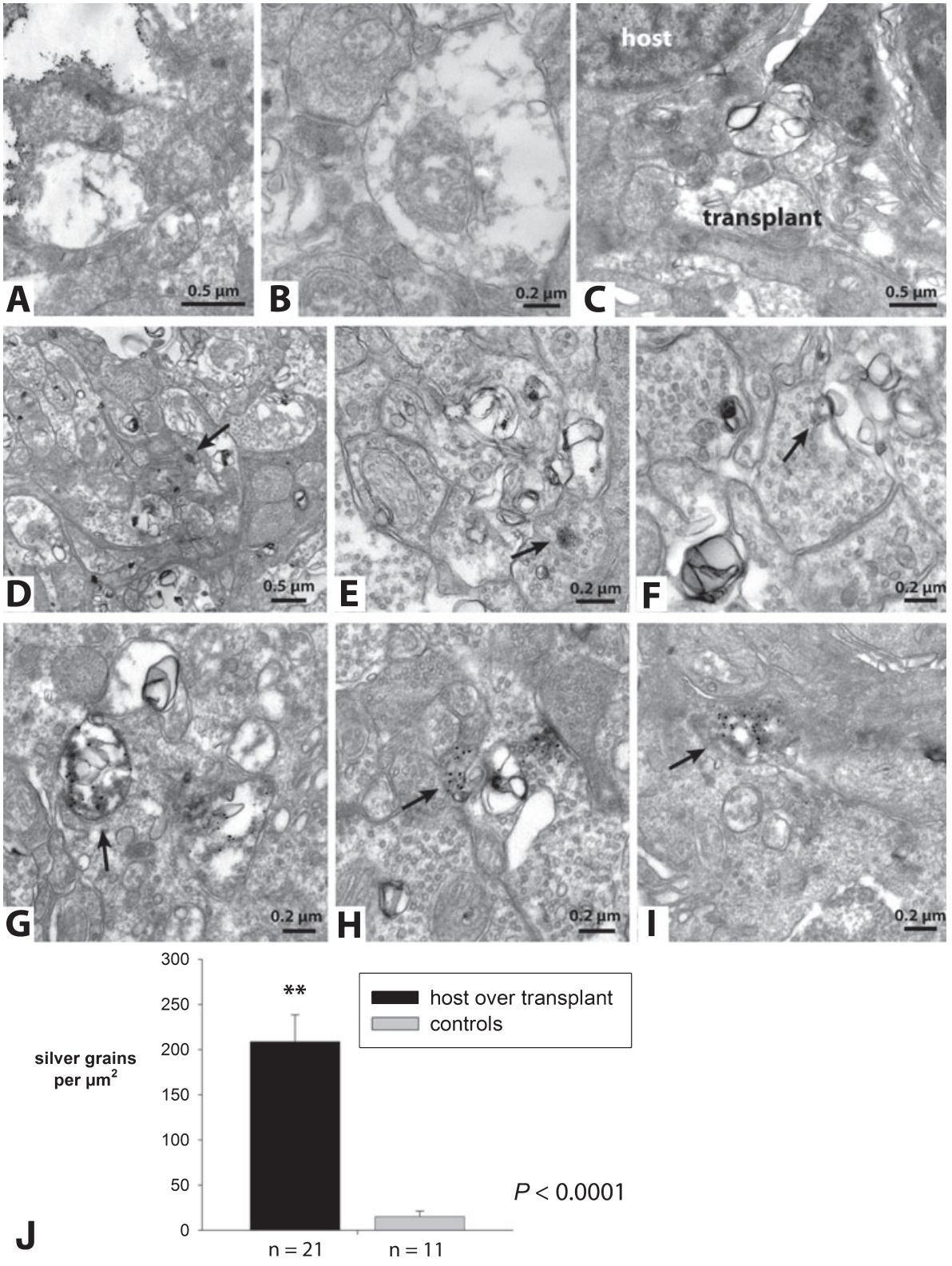
FIG. 5. Examples of controls in the electron microscope. Unspecific silver grains can be seen as edge stain in A, and are indicated by arrows in D–I. This unspecific stain is clearly different from the specific stain shown in Figs. 6 and 7. (A–C) Omission of primary antibody (blocking serum control, rat 11). (D–F) Host retina outside transplant area, stained with human placental alkaline phosphatase (hPAP) antibody 8B6 (rat 9). (G–I) Non-surgery fellow eye, stained with hPAP antibody MAB102 (rat 12). (J) Silver grains in selected images of the host inner plexiform layer over transplants in hPAP stained slices and controls were counted by two independent observers. The results were averaged and expressed as silver grains$/\mu m^2$. Error bars indicate standard errors of the mean.
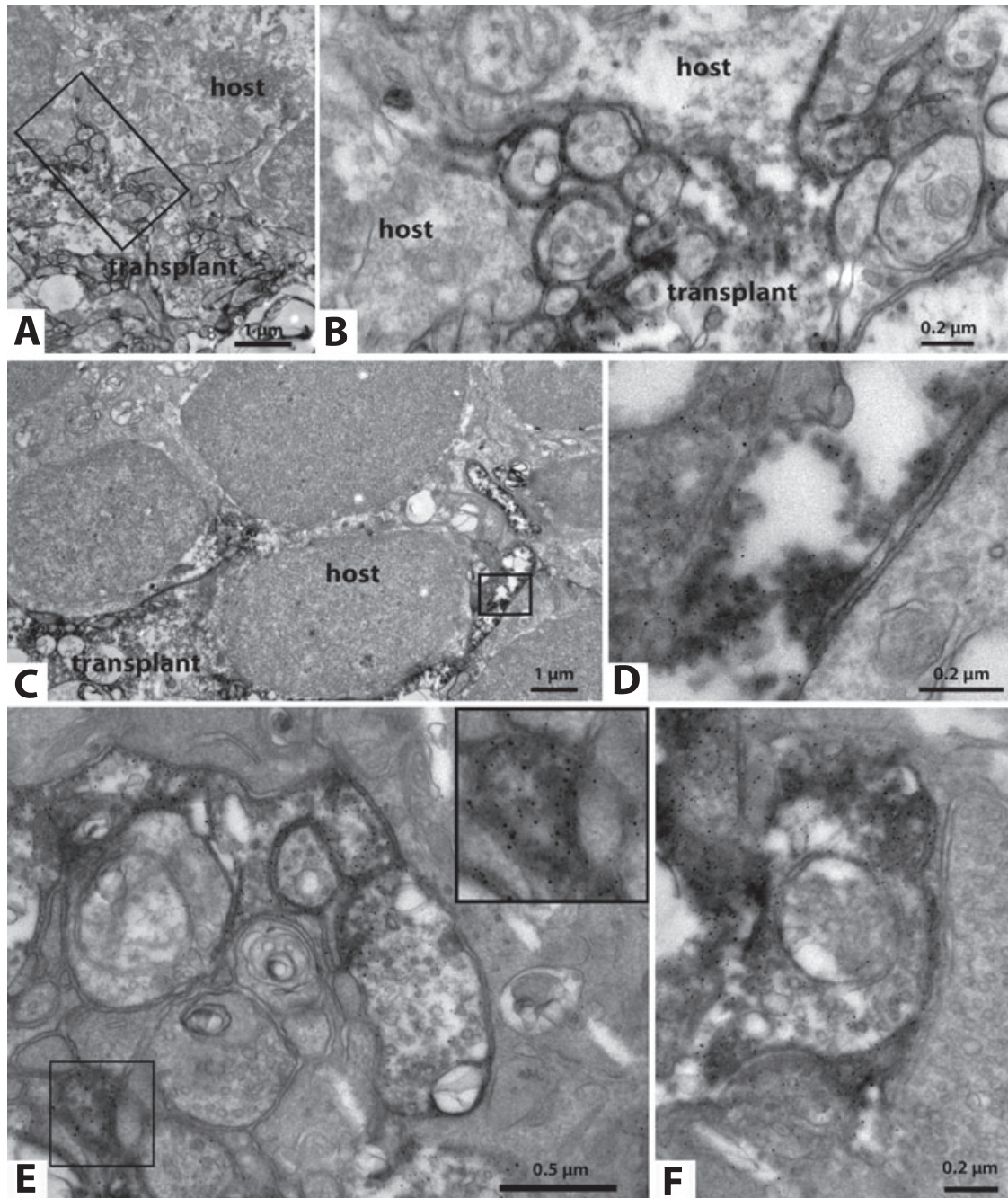
FIG. 6. Processes at the transplant–host interface (electron microscopy). The human placental alkaline phosphatase immunolabel can be recognized as darkness at lower magnification (A and C), and is confirmed by silver grains (dark dots) at high magnification (B and D–F). Note transplant processes extending into the inner nuclear layer of the host retina (A–D). Boxes in A and C indicate areas of enlargement in B and D, respectively. (E and F) Labeled transplant processes in close contact with unlabeled processes of (presumably) host cells. The box in E shows the enlarged process in the insert. (A) Low-power overview (rat 10). (B) Enlargement. Absence of silver grains in the host tissue. (C and D) Rat 13. (E and F) Rat 11. Bars: 1 μm (A and C), 0.5 μm (E), and 0.2 μm (B, D and F).

responses had longer latencies than those from normal rats. Non-transplanted or sham surgery S334ter-3 rats only responded to much stronger light intensities (0 to -1.0 log cd/m^2), with much longer latencies and lower amplitudes at the age of 2.4–3 months, and not later (Thomas *et al.*, 2006). It has been proposed that visual responses of transplanted rats are solely due to a rescue effect of the transplant on host cells (MacLaren & Pearson, 2007). However, we have shown that in rats with visual responses in the SC, retinal sheet transplants do not rescue host cones (Seiler *et al.*, 2008a). In that study, the degenerating host retina overlying the transplant did not contain more red–green

opsin-immunoreactive cones than the host retina outside the graft. In one experimental group, significantly fewer cones were found in the host retinas over the transplant. In all experiments, the visual responses in the SC were limited to areas corresponding to the position of the transplant in the host retina (Seiler *et al.*, 2008a). This was in contrast to the results of another group using rod sheet transplants in the rd mouse model, which showed a rescue effect of the transplant on host cones (Mohand-Said *et al.*, 2000), similar to our results obtained in the same mouse model using retinal progenitor sheet transplants (Arai *et al.*, 2004).
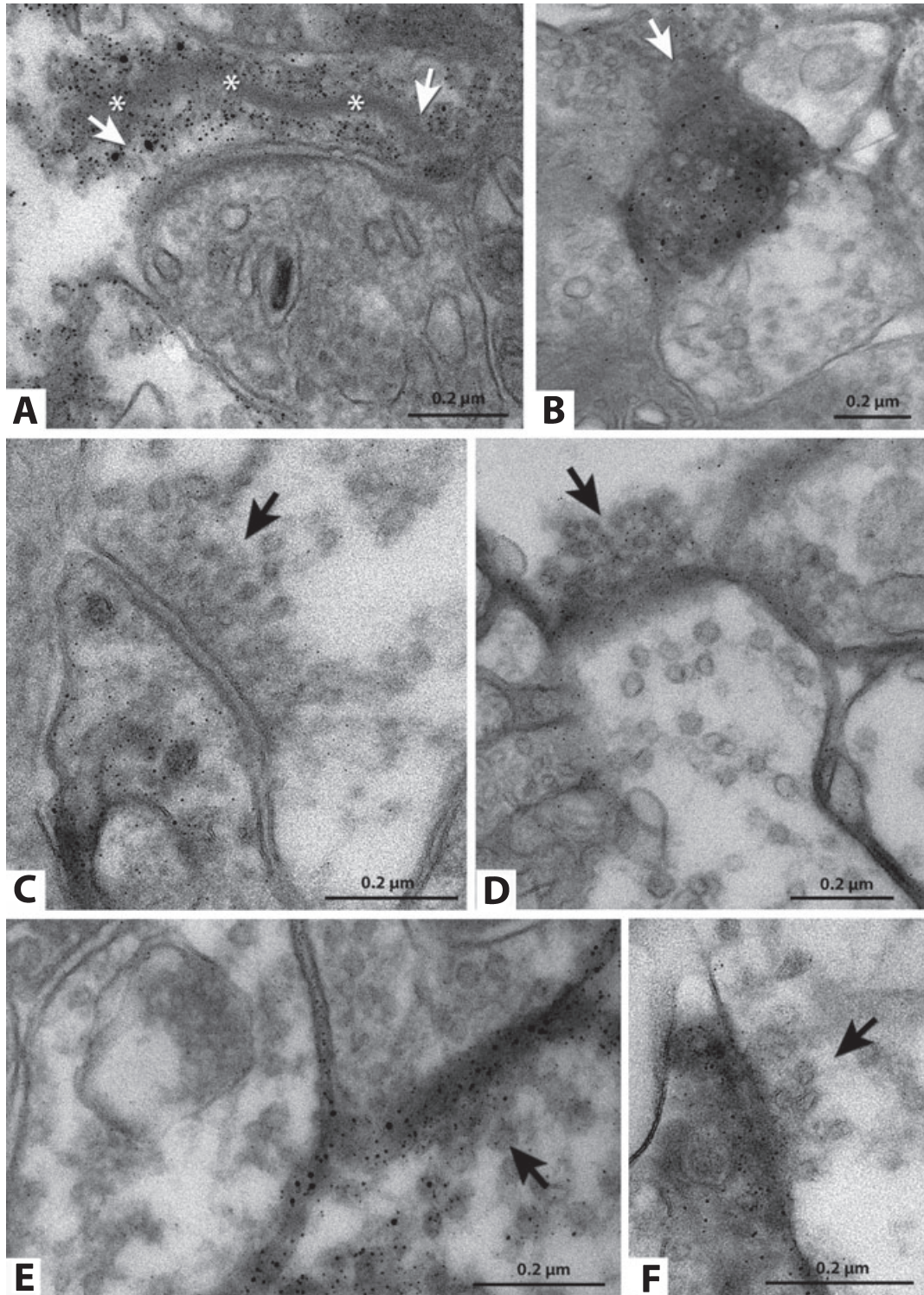
FIG. 7. Transplant processes and synapses in the inner plexiform layer of the host retina. Immunohistochemistry for human placental alkaline phosphatase, recognizable as silver grains. Arrows indicate a presynaptic element of an apparent synapse between transplant and host cell. (A) Labeled ribbon synapse. A long synaptic ribbon is indicated by asterisks. Labeled processes are presynaptic in A, D and E, and postsynaptic in B, C and F. (A and E) Rat 6. (B) Rat 13. (C) Rat 10. (D and F) Rat 8. Bars: 0.2 μm.

The present study is the first to combine SC recordings with ultrastructural analysis of donor cell label. Kwan *et al.* (1999) transplanted retinal microaggregates of neonates to old rd mice, and demonstrated that transplantation affected the light–dark preference of the recipient mice. They found evidence for the formation of an additional synaptic layer at the transplant–host interface at 2.5 weeks after transplantation, but lacked a label for donor cells. Gouras & Tanabe (2003) transplanted microaggregates of newborn retinal cells

from a donor mouse strain expressing *E. coli* beta-galactosidase in rod photoreceptors to an rd mouse strain expressing *E. coli* beta-galactosidase in rod bipolar cells, and analysed their results by electron microscopy. They observed close non-synaptic contacts between donor rods and recipient bipolar cells, and extensions of glial, rather than neuronal, processes between transplant and host. They suggested that those close membrane contacts could provide an indirect means of communication between transplant and host neurons, which could be mediated through the retina to the brain, and which, according to them, could explain the 'weak and delayed' visual responses seen in different transplant models (Radner *et al.*, 2001; Woch *et al.*, 2001). However, with our retinal sheet transplant model, we have seen robust – although delayed – visual responses in different retinal degeneration models. In the S334ter-3 rat model, we have demonstrated that synapses are involved in the visual responses from the SC of transplanted rats, and that the degree of trans-synaptic labeling of the transplant from the host SC is correlated with the visual threshold in SC recordings (Seiler *et al.*, 2008b). The current study is very different, both in design and in methodology, from the previous trans-synaptic studies (Seiler *et al.*, 2005, 2008b), which showed indirect evidence of synapses by injection of pseudorabies virus into the visual responsive site of the SC. The current study shows direct evidence of transplant processes penetrating into the host retina and label at the electron microscopic level.

The ability of retinal progenitor cell transplants to connect and integrate into a degenerative host retina has been questioned. MacLaren *et al.* demonstrated that only postnatal stages of dissociated retinal progenitor cells, expressing the photoreceptor precursor marker Nrl, integrated into the retina, to a very limited extent (0.1–0.3% of transplanted cells), following transplantation (MacLaren *et al.*, 2006; MacLaren & Pearson, 2007). However, their study was not comparable, because it was conducted using dissociated cells, and the mouse models that MacLaren used were different from our rat model. In our study, we found evidence of numerous neuronal processes from the transplant penetrating the inner plexiform layer of the host retina. No such staining was found in slices taken far away from the transplant, or in non-surgery eyes that were stained with the same antibodies. Supporting previous trans-synaptic tracing studies (Seiler *et al.*, 2005, 2008b), our current results indicate that the connectivity with the host occurs via the inner retinal cells of the transplanted fetal retinal sheet (bipolar cells, horizontal cells, amacrine cells, etc.), and not through direct connections of transplant photoreceptors with host cells. However, very few ribbon synapses could be demonstrated that would indicate synapses of photoreceptors or bipolar cells. Preliminary data from another study indicate that any major communication between host and transplant is likely to involve amacrine cells, both glycinergic and GABAergic. Such synapses would not involve classic ribbon synapses.

One shortfall of our study is that we did not use the hPAP antibody in combination with synaptic markers at the electron microscopic level. We have stained previously for synaptic markers at the light microscopic level, using synaptic markers on sections adjacent to hPAP-stained sections (e.g. Seiler *et al.*, 2008a), but it would not have been compatible with the tissue processing for electron microscopy in this study. Therefore, a parallel set of animals was processed for immunohistochemistry and confocal analysis of a combination of donor cell and synaptic markers. Most of the markers used label presynaptic structures. For example, synapsin 1, syntaxin and synaptophysin are all elements of synaptic vesicles. Syntaxin 1 is a synaptosome-associated protein receptor protein that is expressed in conventional synapses and along amacrine cell processes and cell bodies (Barnstable *et al.*, 1985; Sherry *et al.*, 2006). Synapsins regulate the reserve pool of synaptic vesicles (Gitler *et al.*, 2004).

mGluR6 is a specific receptor in on-bipolar cells [reviews: Duvoisin *et al.* (2005) and Snellman *et al.* (2008)]. Bassoon is a cytomatrix component in the active synaptic zone, and is found in the retina in photoreceptor ribbon and amacrine conventional synapses, not in bipolar ribbon synapses (Brandstatter *et al.*, 1999; tom Dieck *et al.*, 2005). Photoreceptor synaptic transmission is severely disturbed in bassoon knockout mice (Dick *et al.*, 2003).

The confocal and electron microscopic data indicate that transplant processes were both presynaptic and postsynaptic to hPAP-negative, presumably host, cells. At the transplant–host interface in the host outer plexiform layer, there was only partial colocalization of transplant processes with synapsin and synaptophysin. Syntaxin immunoreactivity appeared to overlap much more, suggesting that many of the extending transplant processes were derived from amacrine cells. This fits with the observation that few hPAP-labeled ribbon synapses were found at the transplant–host interface by electron microscopy. Transplant processes were seen directly adjacent to synaptophysin-labeled and mGluR6-labeled structures, indicating that they were postsynaptic, but also directly adjacent to PSD95-labeled structures, indicating that they were presynaptic.

During the progression of photoreceptor degeneration in the host retina, other retinal cell types also become affected. The inner retina responds with progressive remodeling, formation of new synaptic circuits, rewiring, and cell death (Jones *et al.*, 2003; Strettoi *et al.*, 2003; Jones & Marc, 2005) [for a review, see Marc *et al.* (2007)]. As our transplants were performed in an early stage of this process, it is conceivable that the recipient's cells were particularly receptive to new contacts from the healthy, actively differentiating transplant cells.

In summary, our data indicate that visual responses in the SC were restored in a rodent model of retinal degeneration following subretinal transplantation of retinal progenitor cell layers. Importantly, visual restoration was correlated with the presence of donor cells and donor processes that penetrated the inner host plexiform layer. This is the first indisputable demonstration of synapse formation between the host and transplant in this system, shown by confocal and electron microscopy.

Acknowledgements

Abbreviations

DAB, diaminobenzidine tetrahydrochloride; EM, electron microscopy; hPAP, human placental alkaline phosphatase; mGluR6, metabotropic glutamate receptor 6; PB, phosphate buffer; PBS, phosphate-buffered saline; SC, superior colliculus.

References

Arai, S., Thomas, B.B., Seiler, M.J., Aramant, R.B., Qiu, G., Mui, C., de Juan, E. & Sadda, S.R. (2004) Restoration of visual responses following transplantation of intact retinal sheets in rd mice. *Exp. Eye Res.*, **79**, 331–341.

Aramant, R.B. & Seiler, M.J. (2002) Retinal transplantation – advantages of intact fetal sheets. *Prog. Retin. Eye Res.*, **21**, 57–73.

Barnstable, C.J., Hofstein, R. & Akagawa, K. (1985) A marker of early amacrine cell development in rat retina. *Brain Res.*, **352**, 286–290.

Brandstatter, J.H., Fletcher, E.L., Garner, C.C., Gundelfinger, E.D. & Wassle, H. (1999) Differential expression of the presynaptic cytomatrix protein bassoon among ribbon synapses in the mammalian retina. *Eur. J. Neurosci.*, **11**, 3683–3693.

Dick, O., tom Dieck, S., Altrock, W.D., Ammermuller, J., Weiler, R., Garner, C.C., Gundelfinger, E.D. & Brandstatter, J.H. (2003) The presynaptic active zone protein bassoon is essential for photoreceptor ribbon synapse formation in the retina. *Neuron*, **37**, 775–786.

tom Dieck, S., Altrock, W.D., Kessels, M.M., Qualmann, B., Regus, H., Brauner, D., Fejtova, A., Bracko, O., Gundelfinger, E.D. & Brandstatter, J.H. (2005) Molecular dissection of the photoreceptor ribbon synapse: physical interaction of Bassoon and RIBEYE is essential for the assembly of the ribbon complex. *J. Cell Biol.*, **168**, 825–836.

Duvoisin, R.M., Morgans, C.W. & Taylor, W.R. (2005) The mGluR6 receptors in the retina: analysis of a unique G-protein signaling pathway. *Cell Sci. Rev.*, **2**, 225.

Gitler, D., Takagishi, Y., Feng, J., Ren, Y., Rodriguiz, R.M., Wetsel, W.C., Greengard, P. & Augustine, G.J. (2004) Different presynaptic roles of synapsins at excitatory and inhibitory synapses. *J. Neurosci.*, **24**, 11368–11380.

Gouras, P. & Tanabe, T. (2003) Survival and integration of neural retinal transplants in rd mice. *Graefes Arch. Clin. Exp. Ophthalmol.*, **241**, 403–409.

Hakamata, Y., Tahara, K., Uchida, H., Sakuma, Y., Nakamura, M., Kume, A., Murakami, T., Takahashi, M., Takahashi, R. & Hirabayashi, M. (2001) Green fluorescent protein-transgenic rat: a tool for organ transplantation research. *Biochem. Biophys. Res. Commun.*, **286**, 779–785.

Humayun, M.S., Prince, M., de Juan, E. Jr, Barron, Y., Moskowitz, M., Klock, I.B. & Milam, A.H. (1999) Morphometric analysis of the extramacular retina from postmortem eyes with retinitis pigmentosa. *Invest. Ophthalmol. Vis. Sci.*, **40**, 143–148.

Jager, R.D., Mieler, W.F. & Miller, J.W. (2008) Age-related macular degeneration. *N. Engl. J. Med.*, **358**, 2606–2617.

Jones, B.W. & Marc, R.E. (2005) Retinal remodeling during retinal degeneration. *Exp. Eye Res.*, **81**, 123–137.

Jones, B.W., Watt, C.B., Frederick, J.M., Baehr, W., Chen, C.K., Levine, E.M., Milam, A.H., LaVail, M.M. & Marc, R.E. (2003) Retinal remodeling triggered by photoreceptor degenerations. *J. Comp. Neurol.*, **464**, 1–16.

Kalloniatis, M. & Fletcher, E.L. (2004) Retinitis pigmentosa: understanding the clinical presentation, mechanisms and treatment options. *Clin. Exp. Optom.*, **87**, 65–80.

Kennan, A., Aherne, A. & Humphries, P. (2005) Light in retinitis pigmentosa. *Trends Genet.*, **21**, 103–110.

Kisseberth, W.C., Brettingen, N.T., Lohse, J.K. & Sandgren, E.P. (1999) Ubiquitous expression of marker transgenes in mice and rats. *Dev. Biol.*, **214**, 128–138.

Kwan, A.S., Wang, S. & Lund, R.D. (1999) Photoreceptor layer reconstruction in a rodent model of retinal degeneration. *Exp. Neurol.*, **159**, 21–33.

MacLaren, R.E. & Pearson, R.A. (2007) Stem cell therapy and the retina. *Eye*, **21**, 1352–1359.

MacLaren, R.E., Pearson, R.A., MacNeil, A., Douglas, R.H., Salt, T.E., Akimoto, M., Swaroop, A., Sowden, J.C. & Ali, R.R. (2006) Retinal repair by transplantation of photoreceptor precursors. *Nature*, **444**, 203–207.

Mahoney, M.J. & Saltzman, W.M. (2001) Transplantation of brain cells assembled around a programmable synthetic microenvironment. *Nat. Biotechnol.*, **19**, 934–939.

Marc, R.E., Jones, B.W., Anderson, J.R., Kinard, K., Marshak, D.W., Wilson, J.H., Wensel, T. & Lucas, R.J. (2007) Neural reprogramming in retinal degeneration. *Invest. Ophthalmol. Vis. Sci.*, **48**, 3364–3371.

Milam, A.H., Li, Z.Y. & Fariss, R.N. (1998) Histopathology of the human retina in retinitis pigmentosa. *Prog. Retin. Eye Res.*, **17**, 175–205.

Mohand-Said, S., Hicks, D., Dreyfus, H. & Sahel, J.A. (2000) Selective transplantation of rods delays cone loss in a retinitis pigmentosa model. *Arch. Ophthalmol.*, **118**, 807–811.

Papermaster, D. & Windle, J. (1995) Death at an early age. Apoptosis in inherited retinal degenerations. *Invest. Ophthalmol. Vis. Sci.*, **36**, 977–983.

Peng, Q., Thomas, B.B., Aramant, R.B., Chen, Z., Sadda, S.R. & Seiler, M.J. (2007) Structure and function of embryonic rat retinal sheet transplants. *Curr. Eye Res.*, **32**, 781–789.

Radner, W., Sadda, S.R., Humayun, M.S., Suzuki, S., Melia, M., Weiland, J. & de Juan, E. Jr (2001) Light-driven retinal ganglion cell responses in blind rd mice after neural retinal transplantation. *Invest. Ophthalmol. Vis. Sci.*, **42**, 1057–1065.

Sagdullaev, B.T., Aramant, R.B., Seiler, M.J., Woch, G. & McCall, M.A. (2003) Retinal transplantation-induced recovery of retinotectal visual function in a rodent model of retinitis pigmentosa. *Invest. Ophthalmol. Vis. Sci.*, **44**, 1686–1695.

Santos, A., Humayun, M.S., de Juan, E. Jr, Greenburg, R.J., Marsh, M.J., Klock, I.B. & Milam, A.H. (1997) Preservation of the inner retina in retinitis pigmentosa. A morphometric analysis. *Arch. Ophthalmol.*, **115**, 511–515.

Seiler, M.J. & Aramant, R.B. (1998) Intact sheets of fetal retina transplanted to restore damaged rat retinas. *Invest. Ophthalmol. Vis. Sci.*, **39**, 2121–2131.

Seiler, M.J., Sagdullaev, B.T., Woch, G., Thomas, B.B. & Aramant, R.B. (2005) Transsynaptic virus tracing from host brain to subretinal transplants. *Eur. J. Neurosci.*, **21**, 161–172.

Seiler, M.J., Thomas, B.B., Chen, Z., Arai, S., Chadalavada, S., Mahoney, M.J., Sadda, S.R. & Aramant, R.B. (2008a) BDNF-treated retinal progenitor sheets transplanted to degenerate rats: improved restoration of visual function. *Exp. Eye Res.*, **86**, 92–104.

Seiler, M.J., Thomas, B.B., Chen, Z., R., W., Sadda, S.R. & Aramant, R.B. (2008b) Retinal transplants restore visual responses – trans-synaptic tracing from visually responsive sites labels transplant neurons. *Eur. J. Neurosci.*, **28**, 208–220.

Sherry, D.M., Mitchell, R., Standifer, K.M. & du Plessis, B. (2006) Distribution of plasma membrane-associated syntaxins 1 through 4 indicates distinct trafficking functions in the synaptic layers of the mouse retina. *BMC Neurosci.*, **7**, 54.

Snellman, J., Kaur, T., Shen, Y. & Nawy, S. (2008) Regulation of ON bipolar cell activity. *Prog. Retin. Eye Res.*, **27**, 450–463.

Strettoi, E., Pignatelli, V., Rossi, C., Porciatti, V. & Falsini, B. (2003) Remodeling of second-order neurons in the retina of rd/rd mutant mice. *Vision Res.*, **43**, 867–877.

Teclemariam-Mesbah, R., Wortel, J., Romijn, H.J. & Buijs, R.M. (1997) A simple silver–gold intensification procedure for double DAB labeling studies in electron microscopy. *J. Histochem. Cytochem.*, **45**, 619–621.

Thomas, B.B., Seiler, M.J., Sadda, S.R. & Aramant, R.B. (2004) Superior colliculus responses to light – preserved by transplantation in a slow degeneration rat model. *Exp. Eye Res.*, **79**, 29–39.

Thomas, B.B., Aramant, R.B., Sadda, S.R. & Seiler, M.J. (2005) Light response differences in the superior colliculus of albino and pigmented rats. *Neurosci. Lett.*, **385**, 143–147.

Thomas, B.B., Aramant, R.B., Sadda, S.R. & Seiler, M.J. (2006) Retinal transplantation – a treatment strategy for retinal degenerative diseases. In Hollyfield, J.G., Anderson, R.E. & LaVail, M.M. (Eds), *Retinal Degenerative Diseases*. Springer, New York, NY, pp. 367–376.

Woch, G., Aramant, R.B., Seiler, M.J., Sagdullaev, B.T. & McCall, M.A. (2001) Retinal transplants restore visually evoked responses in rats with photoreceptor degeneration. *Invest. Ophthalmol. Vis. Sci.*, **42**, 1669–1676.

Zarbin, M.A. (2004) Current concepts in the pathogenesis of age-related macular degeneration. *Arch. Ophthalmol.*, **122**, 598–614.